Numerical Simulation of Turbulent Flow over a Wavy Boundary

CARSTEN MAASS and ULRICH SCHUMANN
DLR, Institute of Atmospheric Physics
D-82230 Oberpfaffenhofen, Germany

Abstract. A wavy wall introduces disturbances into the flow which affect the various quantities describing the mean and temporal fields and the exchange rates at the surface. The main aim of this investigation is the identification of the kind of structures that are produced due to the influence of shear and the wavy wall. Results are presented from direct numerical simulations for a flow in a plane channel with wavy lower and flat top surface. Both surfaces are smooth. The lower surface wave amplitude is 0.05 and the wavelength is 1 in terms of mean channel depth. The Reynolds number in terms of mean velocity and channel depth is 4780. The simulation is in good accordance with the experimental data although the resolution with $160 \times 80 \times 64$ grid points is still too coarse to resolve the very steep velocity gradients at the surface. The effective friction velocity is about 45% larger at the wavy lower surface than at the flat upper surface.

Introduction

Many natural and technical surfaces consist of waves. The wavy wall introduces disturbances into the flow which affect the various quantities describing the mean and temporal fields. If one neglects friction and turbulence, i. e. considers a potential flow with constant mean streamwise velocity, the pressure variation at the surface is 180° out of phase with the wave, and the disturbances decay exponentially with distance from the wall (Lamb [11]). Benjamin [1], using a curvilinear coordinate system, included friction and a mean boundary-layer velocity profile. He showed that the shear layer causes a phase shift of the velocity distribution that produces a drag. Thorsness et al. [13] found a quasi-laminar model sufficient to describe the wall shear stress for wavenumbers $2\pi\nu/(u_\tau\lambda) > 0.01$, but for smaller wavenumbers, the prediction of the phase shift is rather poor. Turbulence models using the van Driest function produce results which agree better with experiments (Kuzan et. al. [10]). For small amplitudes δ and large wavelength λ the flow responds linearly to sinusoidal disturbances. For large enough amplitudes the positive pressure gradient behind the wave is sufficient to cause separation. The flow over a train of waves differs from other separated flows (Dianat and Castro [4]) because the separation which may occur behind each wave crest affects the flow over the following waves.

All these models can describe some properties of the flow but no details of the separation. Recently, Hino and Okumura [7] presented a direct numerical simulation (DNS) of channel flow above mild waviness ($\delta/\lambda = 0.0092$) without separation. The waviness has little effect on the total bottom drag. They found stronger coherent eddy motion on the wavy wall than on the flat

P.R. Voke et al. (eds.), Direct and Large-Eddy Simulation I, 287–297.

wall. The shear-stress distribution showed quasi-stationary streaky patterns corresponding to longitudinal vorticies. Simulations of flows over two- and three-dimensional rough hills have been made by Wood and Mason [14] using a numerical model which employs a $1\frac{1}{2}$-order turbulence closure model. Zilker and Hanratty [16] gave an overview on experimental work, from which the bulk of our understanding of such flows is mainly derived. The experiments concentrated on the measurement of surface pressure, wall shear stress, and velocity components. Motzfeld [12] pointed to the difference between roughness and waviness. Zilker et al. [15] showed that the wall shear stress is a better measure for the linearity of the flow than the velocity.

Buckles et al. [3] found a thin turbulent boundary layer which forms behind the reattachment point and extends to the next separation point. There, a free shear layer develops away from the wall behind the next reattachment point, so that there are now two layers above each other. Gong et al. [6] examined a flow above a wavy wall at two different surface roughnesses. The measurements exhibited an approximately two-dimensional flow with separation over the relatively rough surface. Over the smoother surface they observed a three dimensional secondary flow. The findings can be well modeled by large-eddy simulations (LES). The experiments of Kuzan et al. [10] with $\delta/\lambda = 0.1$ show a decreasing separation with increasing Reynolds number. Recently, Hudson [8] made measurements in a water channel for two different amplitudes and several flow rates. For a case with separation in the mean flow field, he investigated how the Reynolds stresses and turbulence production differ from which what would be observed over a flat wall.

Most theoretical studies were two-dimensional and limited to cases with weak nonlinear effects. Experiments were carried out for a wide set of parameters but not directly comparable and sufficient for turbulence modelling. There is little information about the three-dimensional structures. In this study we investigate the three-dimensional nonlinear flow with moderate Reynolds number by means of DNS and compare the results with the measurements of Hudson [8]. We consider a fixed wavy surface structure, whose wavelength λ is of the same order as the boundary layer thickness. The surface wave amplitude δ is small compared to the boundary layer thickness but too large for linear approximations.

Method

The present numerical method has been used for DNS and LES of turbulent convection over wavy boundaries without (Krettenauer and Schumann [9]) and with mean flow (Dörnbrack and Schumann [5]). But it remains to validate the code for neutral flow because it uses an additional transformation function, contains different boundary conditions, and is applied to a flow with higher requirements on the accuracy of the method because of thinner shear layers at the surface.

The method is explained in detail in Krettenauer and Schumann [9]. The basic equations describe the conservation of mass and momentum for incompressible flows,

$$\frac{\partial u_j}{\partial x_j} = 0, \tag{1}$$

and

$$\frac{\partial u_i}{\partial t} + \frac{\partial}{\partial x_j}(u_j u_i) = -\frac{\partial p}{\partial x_i} + \frac{1}{Re}\frac{\partial^2 u_i}{\partial {x_j}^2} + P_x \delta_{1i}, \qquad i = 1,2,3, \tag{2}$$

where u_i denotes the velocity components, x_i the Cartesian coordinates, t the time, p the deviation from a reference pressure p_0, P_x the driving force in the x-direction and Re the Reynolds number. All quantities are made dimensionless with the channel height H, with the mean streamwise velocity U_m, with the time scale H/U_m and density $\rho = \text{const}$. The equations of motion are formulated for the Cartesian velocity components (u, v, w) as a function of curvilinear coordinates $(\overline{x}, \overline{y}, \overline{z})$ which are related to the Cartesian coordinates according to the transformation $\overline{x} = x$, $\overline{y} = y$, $\overline{z} = \eta(x, y, z)$. Here,

$$\eta = H\frac{z-h}{H-h} \tag{3}$$

maps the domain above the wavy surface at height $h(x, y) = \delta \cos(2\pi x/\lambda)$ and below a plane top surface at $z = H$ onto a rectangular transformed domain. The geometrical parameters are H, the lateral lengths L_x and L_y, the wave amplitude δ, and the wavelength λ, see Figure 1. To get higher resolution at the rigid top and bottom surfaces we use an additional hyperbolical transformation function of a coordinate ξ which is discretized equidistantly,

$$\eta = \frac{H}{2}\left(1 + \frac{\tanh(c\,\xi)}{\tanh c}\right), \quad -1 \le \xi \le 1. \tag{4}$$

The parameter c is choosen so that two adjacent grid spacings $\Delta\eta$ differ by less than 14 %.

The differential equations are approximated by finite differences in a spatial staggered grid. The first discrete grid point for the horizontal velocity components is located $\Delta\eta/2$ above the wall. The momentum equation is integrated in time using the Adams-Bashforth scheme. The mean velocity U_m is defined as the average velocity in the x-direction across a y-z plane at a position with vanishing wave amplitude. After each time step Δt, the actual mean velocity is tested and a mean pressure gradient P_x in the axial direction is determined such that U_m remains constant. At the lateral boundaries, periodicity conditions are used. At the bottom and top surfaces we implement the no-slip condition.

The initial conditions prescribe a laminar velocity profile of a flat channel. Random perturbations are added to the velocity field, which eventually

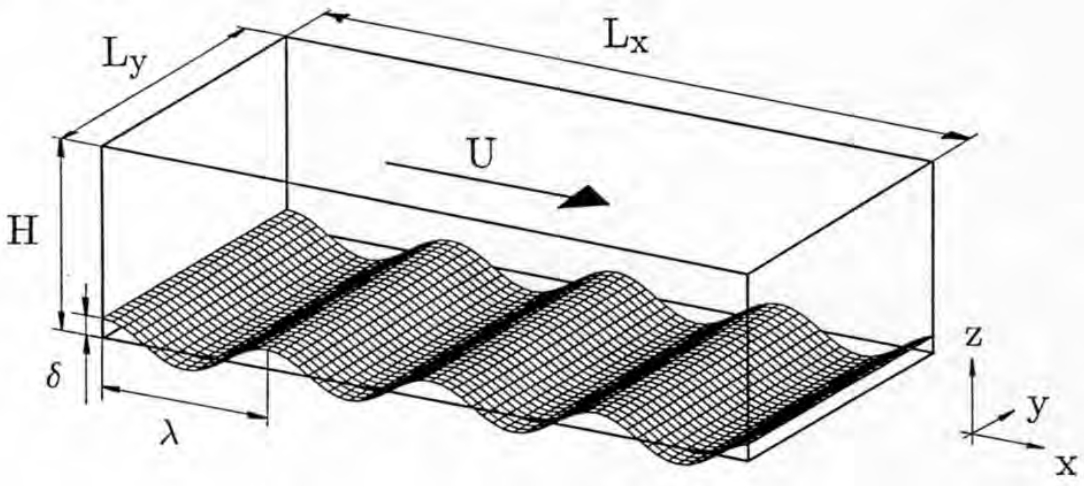

Figure 1. Perspective view of the computational domain in three dimensions showing the sinusoidal surface-wave in x-direction; the surface height is constant in y-direction. In this example, the wavelength is $\lambda = 1$, the wave-amplitude is $\delta = 0.1$, and the domain-size is $H = 1$, $L_x = 4$, and $L_y = 2$.

becomes turbulent. The details of this initialisation are unimportant for the final statistics at late times of the simulation.

We report below results obtained from a set of direct numerical simulations with different resolutions, see Table I. All cases extend over 4 surface wavelengths. The lateral domain size should be large enough to cover the largest turbulent structures. The horizontal grid spacings are equal ($\Delta x = \Delta y$). The vertical grid spacing $\Delta\eta$ is always smaller than the horizontal ones. Case 1 is run with equidistant grid spacing in the vertical. All other cases use variable grid spacings with maximum resolution near the top and bottom surfaces. Using $u_\tau = 0.09\,U_m$, which lies between the bottom and top resultant friction velocities (Table I), the finest resolution in terms of viscous scale is $(\Delta x, \Delta\eta) = (10.8, 2.4)\,\nu/u_\tau$ for case 4. This is still at the limit of what is required to resolve the viscous surface layer. By monitoring the kinetic energy of the whole domain we made sure that the flow is sufficiently stationary at the end of the simulation. All cases are at least run until the final dimensionless time $t = 60$, which for case 4 required 70 000 s CPU time on one processor of a Cray YMP.

Results and Discussion

For comparison with experimental data, the code has been applied for parameters which are the same as used in the laboratory investigations by Hudson [8] in a water channel. The parameters of this experiment are $H = 50.8$ mm,

Table I

Model parameters of the various cases. $\Delta\eta_{min}$ denotes the minimal mesh height, Δt the nondimensional time step, $u_{\tau,fl}$ and $u_{\tau,wa}$ the nondimensional friction velocity at the flat and wavy surface, respectively.

Case	Grid Cells	$L_x \times L_y \times H$	$\Delta\eta_{min}$	Δt	$u_{\tau,fl}$	$u_{\tau,wa}$
1	$80 \times 40 \times 40$	$4 \times 2 \times 1$	0.025	0.01	0.081	0.104
2	$80 \times 40 \times 40$	$4 \times 2 \times 1$	0.008	0.01	0.075	0.106
3	$160 \times 80 \times 48$	$4 \times 2 \times 1$	0.0085	0.006	0.071	0.104
4	$160 \times 80 \times 64$	$4 \times 2 \times 1$	0.0055	0.006	0.070	0.101

$\delta = 2.54$ mm, $\lambda = 50.8$ mm, the mean velocity of the lower half of the channel $U_m = 86.4$ mm/s, and $Re = U_m H/\nu = 4780$. For these parameters, the map of Zilker and Hanratty [16] predicts turbulent flow with mean separation, and the experiment shows that the flow is always turbulent with mean and intermittent flow reversal. The measurements were carried out using laser-Doppler velocimetry (LDV), which results we use here, as well as particle-image velocimetry. The LDV measurements have been taken over a period of 60 s, i. e. 102 H/U_m, with 2 ms between measurements. Hudson [8] determined a mean velocity U_m based solely on the velocity measurements in the lower half of the channel. We used the same value to prescribe the mean flow over the whole channel. It turned out that the computed mean over the lower half of the channel is 7 % smaller than the mean over the whole channel. As a consequence, the Reynolds number is in effect 7 % smaller in the computation than in the experiment. For comparison of velocity results, data of the simulation and from the experiment are made dimensionless with the respective mean velocity of the lower half of the channel.

For the coarsest grid and for equidistant vertical resolution the results do not show a separation. The separation arises only in a transient initial phase but disappears at later times. It turns out that a rather fine resolution near the boundaries is required to correctly simulate the separated region. With grid refinement near the walls the flow separates even with the coarsest grid. If we double the horizontal resolution the result is almost the same. But even with the highest resolution, where $\Delta\eta\, u_{\tau,wa}/(2\nu) = 1.3$, the computed velocity gradients near the wavy surface are smaller than measured. In general the u-velocities are too small near the wavy wall and too large near the center. This can be seen Figure 2 which depicts profiles of the computed and measured streamwise velocity. The largest differences occur near $x/\lambda = 0.8$. The separated region, bounded by the streamline $\Psi = 0$, is about 60% higher than in the experiment and extends from $x/\lambda = 0.2$ to $x/\lambda = 0.63$ which interval is 0.2 larger than in the experiment. Figure 3 shows the averaged (over y and over the 4 waves) velocity field in a vertical plane. It exhibits a regular recir-

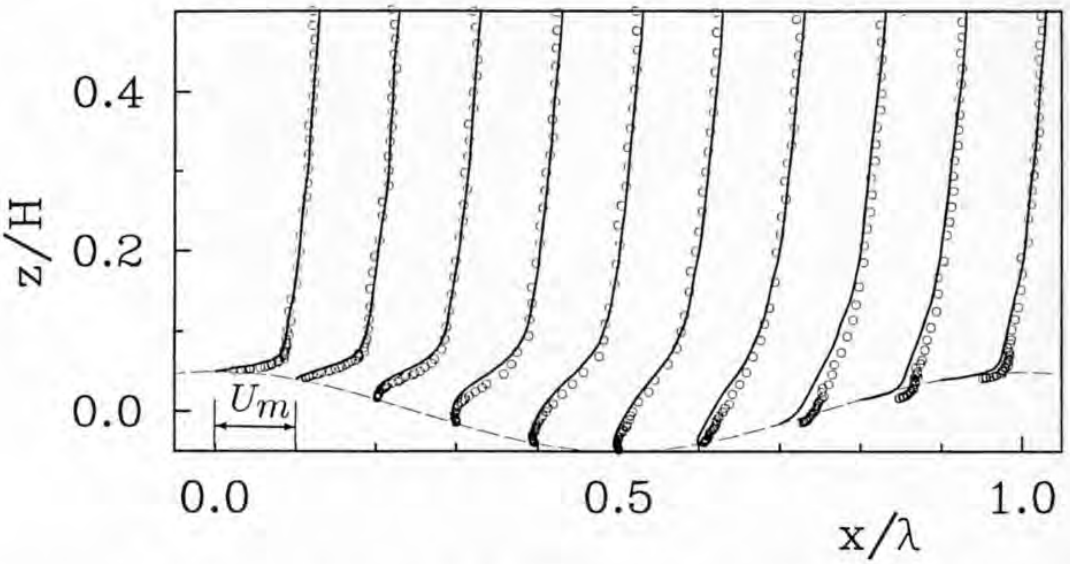

Figure 2. Profiles of mean u-velocity at different streamwise positions. —— spanwise and phase-averaged results of case 4 at $t = 60\,H/U_m$; o time averaged LDV measurements of Hudson. The dashed curve indicates the shape of the surface wave.

culation zone and strong shear over the wave crest. At specific times, more complicated structures arise, see Figure 4. From studying other instantaneous flow fields at various times and spanwise positions, we know that the recirculation zone, which occasionally fills almost the whole trough region, is strongly intermittent and three-dimensional. Further, a small distance downstream of the crest, spanwise eddies can be observed which detach from the wall. On the other hand, the flow above the crests appears to be close to stationary and almost two-dimensional. However, the fluctuating flow field (Figure 5) illuminates that also above the crests three-dimensional perturbations evolve in terms of counterrotating streamwise vortices. These vortices develop behind the reattachment point and extend up to the crest.

Figure 6 shows turbulence variances horizontally averaged at constant values of the coordinate η. The downstream velocity variance has maxima near the surfaces and a minimum near $\eta = 0.7\,H$. The maxima are located $0.05\,H$ and $0.09\,H$ from the upper and lower wall, respectively. For the lowest resolution (case 2) the values near the lower maximum are about 30% higher than in the measurements. With increasing resolution we get a better agreement with deviation from the experiment less than 10% near the maximum. Also the ratio between the lower and the upper variance maxima decreases with increasing resolution. Due to the waviness, the normal velocity variance has a maximum near $\eta = 0.05\,H = 1\,\delta$. Also the spanwise velocity variance is strongly influenced by the wavy wall. Its maximum value is about 1/3 of that of the u-variance. The mean vertical momentum flux vanishes near $\eta = 0.65\,H$.

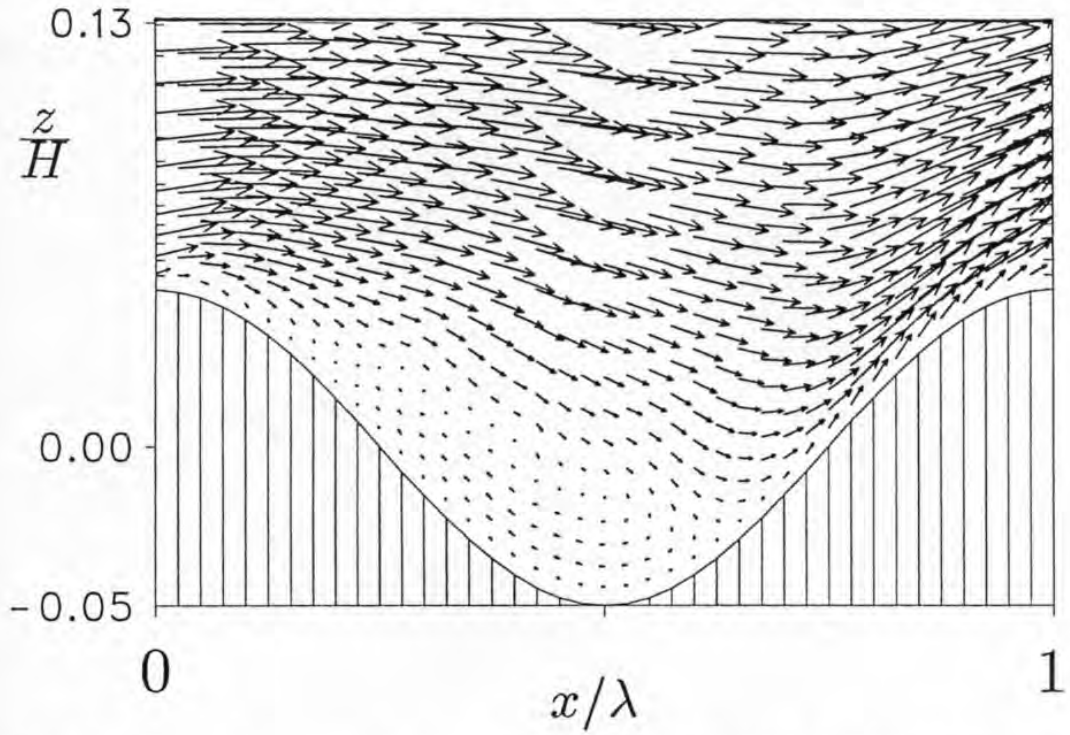

Figure 3. Averaged (over y and over the 4 waves) flow field of case 4 at $t = 60\,H/U_m$.

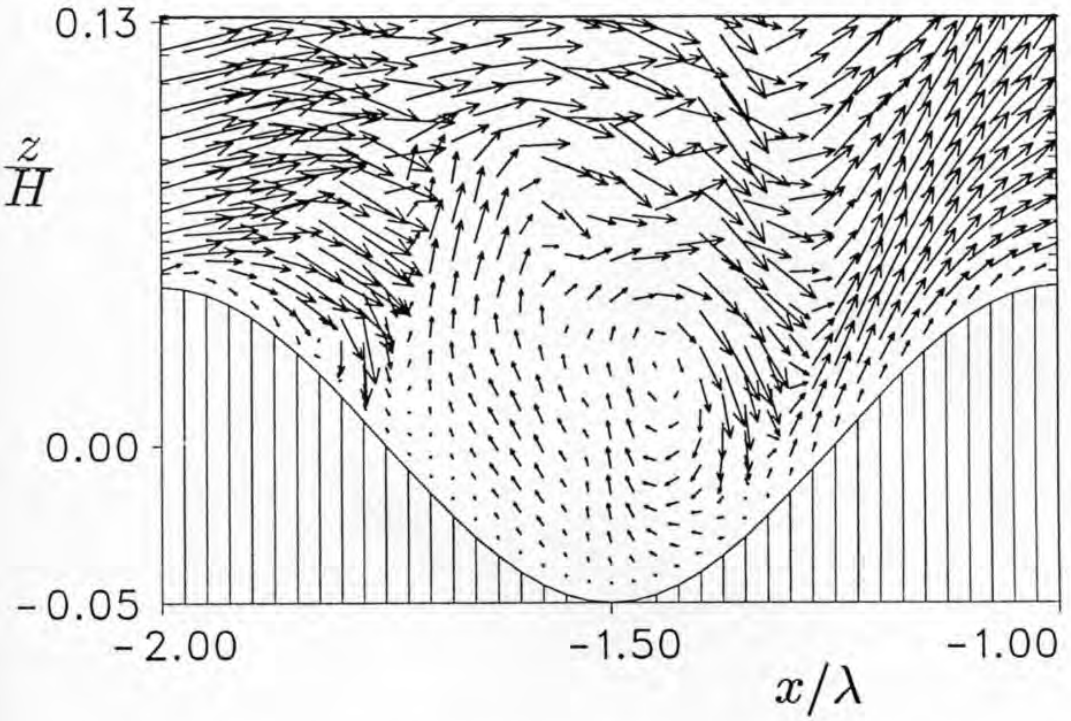

Figure 4. Instantaneous flow field of case 4 at $y = \text{const.}$ $(t = 60\,H/U_m)$.

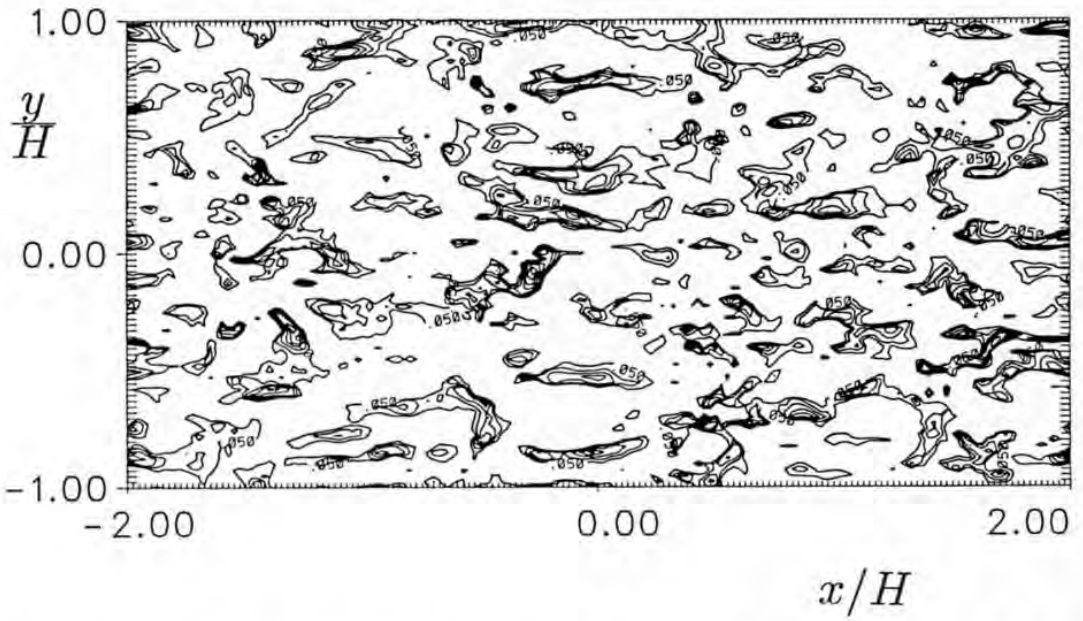

Figure 5. Instantaneous vertical velocity fluctuations of case 4 at $\eta = 0.07$ (i. e. $\eta = 39\,\nu/u_{\tau,wa}$ at the 10th grid level; only positive contours with interval 0.05). The crests of the wavy wall are located at $x = -2, -1, 0, 1, 2\,H$.

The computed profile of the surface pressure (Figure 7 a)), which is responsible for the form drag, has the same shape as in the experiment and does not change much with resolution. The location of its absolute maximum at $x/\lambda = 0.7$ coincides with the reattachment point. This situation is comparable to a jet impinging on a surface. Because of differences in shape and magnitude of the recirculating flow, the computed pressure maximum is about 30% smaller than the experimental value. The latter was obtained indirectly by calculating the pressure field from the velocity field using a reference pressure measured near the channel center. There is also an influence from the fact that the flow feels an effectively lower wave if there is a greater separation. A change of slope in the surface pressure profile appears at $x/\lambda = 0.2$, which is near to the separation point. Apart from small regions around the crest and the reattachment point the pressure is nearly constant in z up to $z = 0.25$.

The vertical flux of downstream momentum τ is composed of advective contributions due to the mean flow field and frictional parts due to turbulent fluctuations. Both contributions are modified by the wavy wall. In addition, at wavy surfaces the pressure causes a further contribution $\tau_{pres} = \overline{p(\partial z/\partial x)_\eta}$, where the bar denotes the horizontal average over coordinate planes $\eta = \text{const}$. In Figure 7 b) we show the different contributions to the total momentum flux. The frictional part is very small near the channel center but considerably large

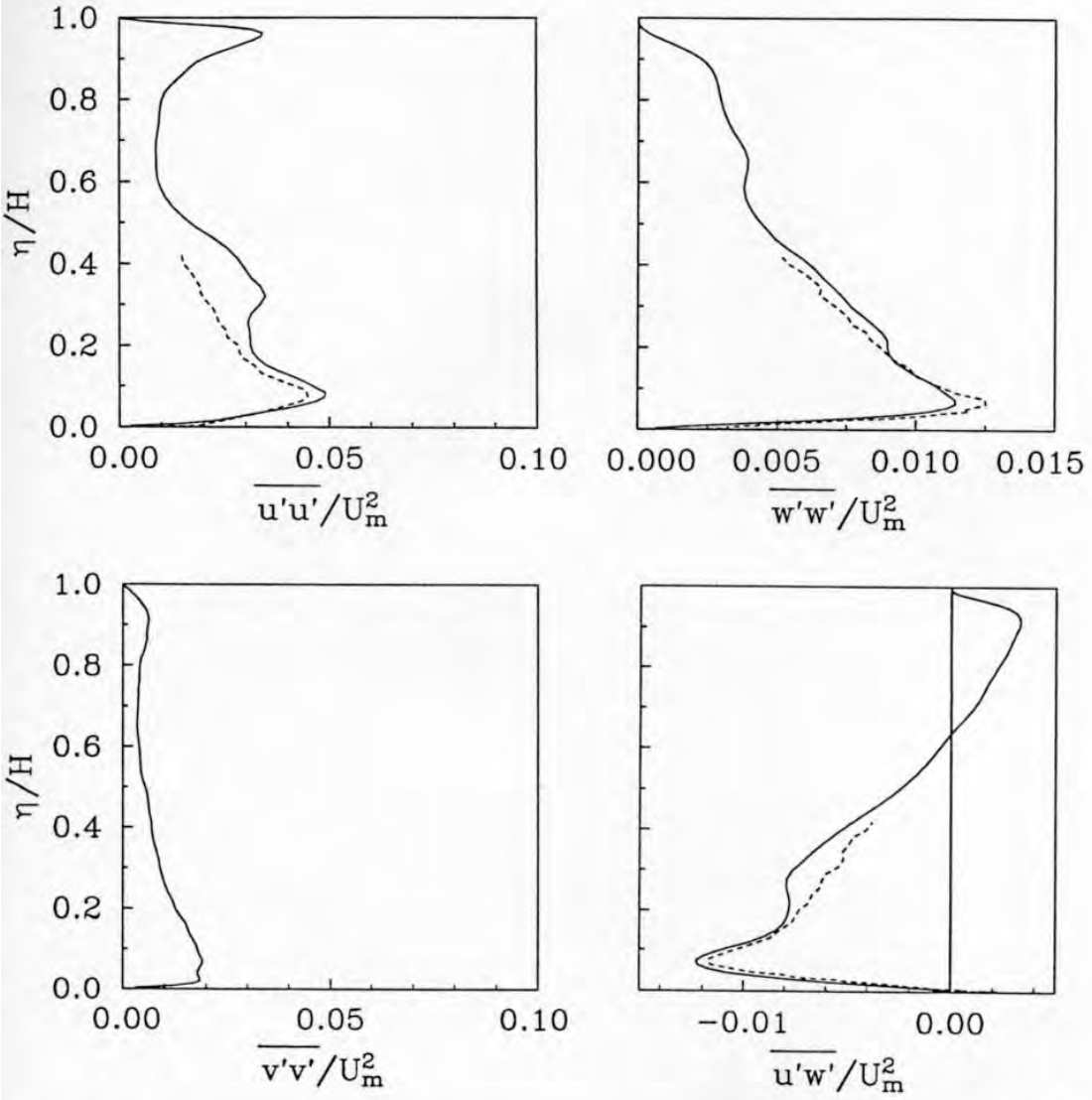

Figure 6. Vertical profiles of mean turbulence variances versus η. —— Case 4 at $t = 60\, H/U_m$; - - - Time averaged LDV measurements of Hudson.

near the walls. At the flat wall, it is the only non-zero contribution, which is 34% higher than at the wavy wall, because of the higher velocities at the flat wall. The advective part which is zero at the surfaces is strongly influenced by the vortical motion induced by the surface waves. This influence reaches almost the channel midheight and causes the deviation from the linear profile in the lower domain of the channel. The pressure contribution is important only near the wavy bottom and exceeds the sum of advectional and frictional momentum transport. The profile of the total momentum flux deviates from

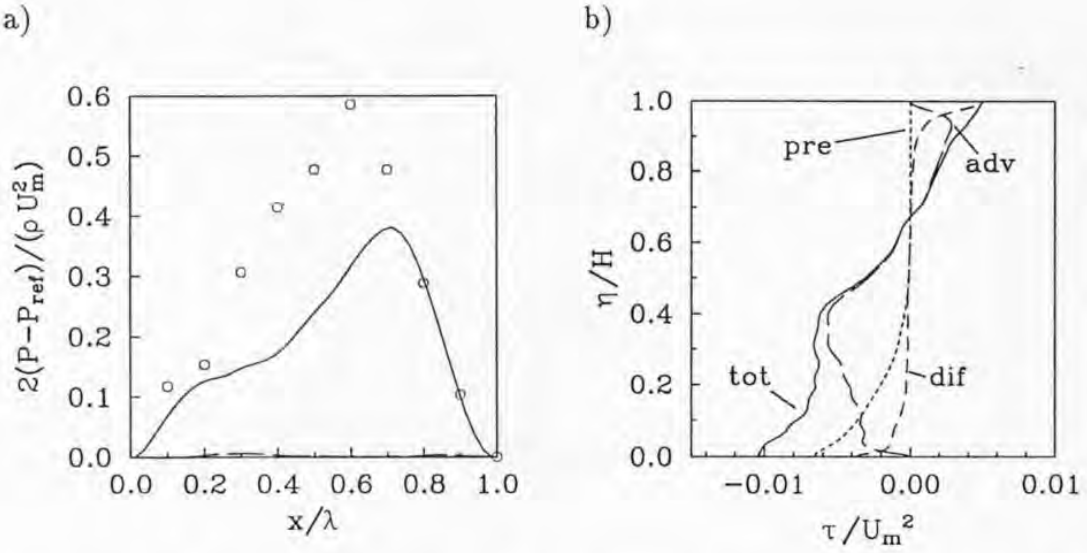

Figure 7. a) Surface pressure along the walls (—— lower wavy wall, - - - - top flat wall, o Hudson (1993)). b) Horizontally averaged vertical flux of downstream momentum at $t = 60\,H/U_m$; dif: frictional contribution; adv: advective contribution; pre: pressure contribution; tot: total momentum flux.

a linear profile due to the influence from the wavy bottom mainly through the advective contribution and the pressure drag. The friction velocities, see Table I, are computed from the total drag.

The computed shear stress distribution at the flat wall shows streaky patterns as observed by Hino and Okumura [7]. On the wavy wall we only find streaky patterns on the upstream slope and less regular patterns of different shape on the downstream slope.

Conclusion

In this study, direct numerical simulations of turbulent flow over a wavy boundary have been carried out and compared to measurements by Hudson [8]. Our method is able to predict the main features of separated flow and the flow structure can be described. In particular we find that a recirculation zone develops. This recirculation could be simulated with a rather coarse grid but only when a variable vertical grid spacing is used with finer resolution of the order ν/u_τ near the walls. Also the computed mean velocity profiles and mean turbulence profiles agree rather well with the measurements. Mainly because of the additional pressure drag, the effective friction velocity is about 45% larger at the wavy lower surface than at the flat upper surface. Near the wavy surface the flow shows a streaky pattern with downstream elongated vortices at the upstream slope but less regular patterns on the downstream side. The size of the separation in the simulation is larger than in the experiment, which

yields a smaller pressure drag. As one possible explanation one might consider a finite surface smoothness in the experiment (Britter et al. [2]). However, since we use an ideally smooth surface, the separation should be smaller in the simulation. On the other hand, the Reynolds number in the simulation, which is a little smaller than in the experiment, may partly explain the larger separation region. However, we expect that an even finer resolution is required in the simulation for complete agreement with the measurements.

References

1. Benjamin, T. B., *Shearing flow over a wavy boundary*. J. Fluid Mech., 6:161–205, 1959.
2. Britter, R. E., J. C. R. Hunt and K. J. Richards, *Air flow over a two-dimensional hill: studies of velocity speed-up, roughness effects and turbulence*. Q. J. R. Meteorol. Soc., 107:91–110, 1981.
3. Buckles, J. J., T. J. Hanratty and R. J. Adrian, *Turbulent flow over large-amplitude wavy surfaces*. J. Fluid Mech., 140:27–44, 1984.
4. Dianat, M. and I. P. Castro, *Turbulence in a separated boundary layer*. J. Fluid Mech., 226:91–123, 1991.
5. Dörnbrack, A. and U. Schumann, *Numerical Simulation of Turbulent Convective Flow over Wavy Terrain*. Boundary-Layer Meteorol., 65:323–355, 1993.
6. Gong, W., P. A. Taylor, and A. Dörnbrack, *Turbulent boundary-layer flow over fixed, aerodynamically rough, 2-d sinusoidal waves*. Boundary-Layer Meteorol., 1994. submitted.
7. Hino, M. and T. Okumura, *Coherent structure of turbulent flow over wavy walls*. In *Proc. 9th Turbulent Shear Flow Symp. Kyoto, Aug. 16-18*, pp. 14.3.1–4, 1993.
8. Hudson, J. D., *The effect of a wavy boundary on turbulent flow*. PhD thesis, Dept. Chemical Engineering, University of Illinois, Urbana, 1993.
9. Krettenauer, K. and U. Schumann, *Numerical simulation of turbulent convection over wavy terrain*. J. Fluid Mech., 237:261–299, 1992.
10. Kuzan, J. D., T. J. Hanratty, and R. J. Adrian, *Turbulent flows with incipient separation over solid waves*. Exper. in Fluids, 7:88–98, 1989.
11. Lamb, H., *Hydrodynamics*. Dover, New York, 1945.
12. Motzfeld, H., *Die turbulente Strömung an welligen Wänden*. Z. angew. Math. Mech., 17:193–212, 1937.
13. Thorsness, C. B., P. E. Morrisroe, and T. J. Hanratty, *A comparison of linear theory with measurements of the variation of shear stress along a solid wave*. Chem. Eng. Sci., 33:579–592, 1978.
14. Wood, N. and P. Mason, *The pressure force induced by neutral, turbulent flow over hills*. Q. J. R. Meteorol. Soc., 119:1233–1267, 1993.
15. Zilker, D. P., G. W. Cook, and T. J. Hanratty, *Influence of the amplitude of a solid wavy wall on a turbulent flow. Part 1. Non-separated flows*. J. Fluid Mech., 82:29–51, 1977.
16. Zilker, D. P. and T. J. Hanratty, *Influence of the amplitude of a solid wavy wall on a turbulent flow. Part 2. Separated flows*. J. Fluid Mech., 90:257–271, 1979.